Full paper

Control and system identification for the Berkeley lower extremity exoskeleton (BLEEX)

JUSTIN GHAN, RYAN STEGER and H. KAZEROONI *

Department of Mechanical Engineering, University of California, Berkeley, CA 94720, USA

Abstract—The Berkeley lower extremity exoskeleton (BLEEX) is an autonomous robotic device whose function is to increase the strength and endurance of a human pilot. In order to achieve an exoskeleton controller which reacts compliantly to external forces, an accurate model of the dynamics of the system is required. In this report, a series of system identification experiments was designed and carried out for BLEEX. As well as determining the mass and inertia properties of the segments of the legs, various non-ideal elements, such as friction, stiffness and damping forces, are identified. The resulting dynamic model is found to be significantly more accurate than the original model predicted from the designs of the robot.

Keywords: BLEEX; exoskeleton; control; system identification.

1. INTRODUCTION

The goal of the exoskeleton project at UC Berkeley is to develop fundamental technologies associated with the design and control of energetically autonomous lower extremity exoskeletons that augment human strength and endurance during locomotion. The first generation lower extremity exoskeleton (commonly referred to as BLEEX) is comprised of two powered anthropomorphic legs, a power unit and a backpack-like frame on which a variety of heavy loads can be mounted. This system provides its pilot (i.e., the wearer) with the ability to carry significant loads on his/her back with minimal effort over any type of terrain. BLEEX allows the pilot to comfortably squat, bend, swing from side to side, twist, and walk on ascending and descending slopes, while also offering the ability to step over and under obstructions while carrying equipment and supplies. BLEEX has numerous potential applications; it can provide soldiers, disaster relief workers, wildfire fighters and other emergency personnel with the ability to carry heavy loads, such

---

*To whom correspondence should be addressed. E-mail: kazerooni@berkeley.edu

Figure 1. BLEEX.

as food, rescue equipment, first-aid supplies, communications gear and weaponry, without the strain typically associated with demanding labour.

BLEEX was first unveiled in 2004, at UC Berkeley's Human Engineering and Robotics Laboratory (Fig. 1). In this initial model, BLEEX offered a carrying capacity of 34 kg (75 lb), with weight in excess of that allowance being supported by the pilot.

The effectiveness of the lower extremity exoskeleton is a direct result of the control system's ability to leverage the human intellect to provide balance, navigation and path-planning while ensuring that the exoskeleton actuators provide most of the strength necessary for supporting payload and walking. In operation, the exoskeleton becomes transparent to the pilot and there is no need to train or learn any type of interface to use the robot.

The control algorithm ensures that the exoskeleton always moves in concert with the pilot with minimal interaction force between the two and was first presented in Ref. [1]. It needs no direct measurements from the pilot or the human–machine interface (e.g., no force sensors between the two). The controller estimates, based on measurements from the exoskeleton structure only, how to move so that the pilot feels very little force. This control scheme is an effective method of generating locomotion when the contact location between the pilot and the exoskeleton is unknown and unpredictable (i.e., the exoskeleton and the pilot are in contact in variety of places).

This control method differs from compliance control methods employed for upper extremity exoskeletons [2−4] and haptic systems [5, 6] because it requires no force sensor between the wearer and the exoskeleton. Taking into account this new approach, our goal was to develop a control system for BLEEX with high sensitivity. Systems with high sensitivity to external forces and torques are not robust to variations, and therefore the precision of the system performance is proportional to the precision of the exoskeleton dynamic model.

The dynamics of the exoskeleton can be predicted theoretically using the simplified model of the robot leg as a three-segment manipulator, with the mass and inertia properties of the robot links predicted from design models. However, a large number of factors affecting the dynamics cannot be predicted from this approach. Many parts of the robot cannot be modeled accurately, e.g., the dynamics of the hosing and wiring, and the internal dynamics of the actuators. Additionally, there are many unknown forces acting within the robot, caused by friction, stiffness and damping of various elements.

Therefore, the model of the robot must be obtained experimentally. This report discusses the identification of the dynamics of a leg of the robot which is not in contact with the ground. This is called the swing mode of the leg, as opposed to the stance mode when the foot is touching the ground. During walking, the motions of a leg while in swing mode are generally faster and larger than those while in stance mode. Therefore, it is more important to have compliancy in the swing mode. For this reason, the system identification was first performed only for swing mode. However, the system identification methods used for the swing mode dynamics could be adapted to be used for the stance mode dynamics.

2. CONTROLLER IMPLEMENTATION

The BLEEX control algorithm, which has been presented in detail in Refs [1, 7], ensures that the exoskeleton always moves in concert with the pilot. In addition, it must maintain minimal interaction force between the two in order to be comfortable and non-fatiguing. The controller needs no direct measurements from the pilot or the human–machine interface (e.g., no force sensors between the two). Instead, it estimates, based on measurements from the exoskeleton structure only, how to move so that the pilot feels very little force. This control scheme is a particularly effective method of generating locomotion when the contact location between the pilot and the exoskeleton is unknown and unpredictable (i.e., the exoskeleton and the pilot are in contact in variety of places).

In order to move with the pilot, the controller must give the exoskeleton a large sensitivity to the small forces and torques applied by the pilot. To achieve this, the exoskeleton controller uses the inverse of the exoskeleton dynamics, G, as a positive feedback such that the loop gain for the exoskeleton approaches unity from below
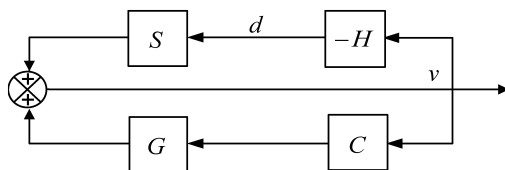
Figure 2. The two feedback loops in this diagram represent the overall motion of the human and exoskeleton (from Ref. [7]). The upper feedback loop shows how the pilot moves the exoskeleton through applied forces. The lower positive feedback loop shows how the controller drives the exoskeleton.

(slightly less than 1). Based on the block diagram in Fig. 2, this can be written as:

$$S_{\text{NEW}} = \frac{v}{d} = \frac{S}{1 - GC},\tag{1}$$

where C is chosen as:

$$C = (1 - \alpha^{-1})G^{-1}\tag{2}$$

and α is the amplification number greater than unity. The sensitivity transfer function, S, represents how the equivalent human torque affects the exoskeleton angular velocity. S maps the equivalent pilot torque, d, onto the exoskeleton velocity, v. The resulting torque from pilot on the exoskeleton, d, is not an exogenous input; it is a function of the pilot dynamics, H, and variables such as position and velocity of the pilot and the exoskeleton legs.

　Figure 2 shows an important characteristic for human exoskeleton control: two distinct feedback loops in the system. The upper feedback loop represents how forces and torques from the pilot affect the exoskeleton and is internal to the human. The lower loop shows how the controlled feedback loop affects the exoskeleton. While the lower feedback loop is positive (potentially destabilizing), the upper human feedback loop stabilizes the overall system of pilot and exoskeleton taken as a whole. This controller, originally discussed in Ref. [7], provides high sensitivity to pilot input and is stable when worn by the pilot provided parameter uncertainties are kept to a minimum. To ensure model accuracy, system identification is employed to accurately obtain model parameters.

2.1. BLEEX mechanical system

BLEEX, as shown in Fig. 1, is a system with many degrees of freedom (d.o.f.) and which requires different dynamic models depending on the ground contact configuration of the left and right legs. Each BLEEX leg has 3 d.o.f. at the hip, 1 d.o.f. at the knee and 3 d.o.f. at the ankle, of which only four are powered d.o.f.: hip, knee and ankle joints in the sagittal plane, and the hip abduction/adduction joints. See Refs [8, 9] for details of the BLEEX mechanical design.

　The pilot and BLEEX have rigid mechanical connections at the torso and the feet; everywhere else, the pilot and BLEEX have compliant or periodic contact. The

connection at the torso is made using an adjustable compliant vest that distributes the forces between BLEEX and the pilot, thereby preventing abrasion. This compliant pilot vest attaches to the rigid metal spine of the BLEEX torso.

The pilot's shoes or boots attach to the BLEEX feet using a modified quick-release binding mechanism similar to snowboard bindings. The binding cleat on the modified pilot boot does not interfere with normal wear when the pilot is unclipped from BLEEX. The BLEEX foot is composed of a rigid heel section with the binding, and a compliant, but load-bearing, toe section that begins mid foot and extends to the toe. The BLEEX foot has a compressible rubber sole with a tread pattern that provides both shockabsorption and traction while walking. The rubber sole of the BLEEX foot contains multiple embedded pressure sensors (digital on/off information) that are used to detect the trajectory of the BLEEX ground reaction force starting from 'heel-strike' to 'toe-off' in the walking gait cycle. This information is used in the BLEEX controller to identify the BLEEX foot configuration relative to the ground and subsequently choose the appropriate model for the BLEEX inverse dynamics.

BLEEX is powered via a compact portable hybrid output power supply contained in the backpack. Several different portable BLEEX power supplies have been designed by our group for different applications and environments. Each provides hydraulic flow and pressure for the actuators, and generates electric power for the sensors, network and control computer. Details of the design, testing and performance of the BLEEX power supplies can be found in Refs [10–12]. A description of the BLEEX control network and electronics can be found in Refs [13, 14].

2.2. Dynamic modeling

We consider BLEEX to have three distinct phases during walking (shown in Fig. 3) which manifest to three different dynamic models (percentage of the gait cycle indicated):

- Single support: one leg is in the stance configuration while another leg is in swing (40% of gait cycle).
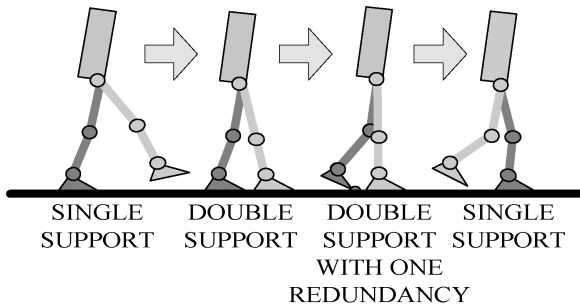

Figure 3. Three phases of the BLEEX walking gait cycle.

- Double support: both legs are in stance configuration and situated flat on the ground (20% of gait cycle).

- Double support with one redundancy: both legs are in stance configuration, but one leg is situated flat on the ground while the other one is not (40% of gait cycle).

Using the information from the sensors in the foot sole, the controller determines which phase BLEEX is operating in and which of the three dynamic models apply.

2.3. Single stance

In the single-support phase, BLEEX is modeled as the 7 d.o.f. serial link mechanism in the sagittal plane as shown in Fig. 4. The dynamics of BLEEX can be written in the general form as:

$$M(\theta)\ddot{\theta} + C(\theta, \dot{\theta})\dot{\theta} + P(\theta) = T + d, \tag{3}$$

where

$$\theta = \begin{bmatrix} \theta_1 \\ \theta_2 \\ \vdots \\ \theta_7 \end{bmatrix}, \quad T = \begin{bmatrix} 0 \\ T_2 \\ \vdots \\ T_7 \end{bmatrix}. \tag{4}$$

$M(\theta)$ is a 7×7 inertia matrix and is a function of θ; $C(\theta, \dot{\theta})$ is a 7×7 centripetal and Coriolis matrix, and is a function of θ and $\dot{\theta}$; and $P(\theta)$ is a 7×1 vector of gravitational torques and is a function of θ only. T is the 7×1 actuator torque vector with its first element set to zero since there is no actuator associated with joint angle θ_1 (i.e., the angle between the BLEEX foot and the ground). d is the effective 7×1 torque vector imposed by the pilot on BLEEX at various locations. According to (2), we choose the controller to be the inverse of the BLEEX dynamics
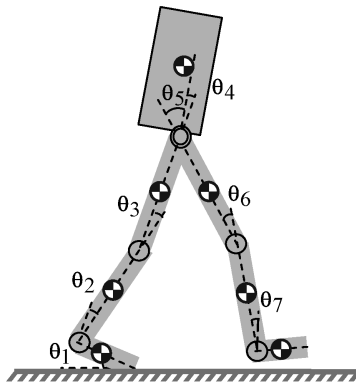

Figure 4. Sagittal plane representation of BLEEX in the single-support phase.

scaled by $(1 - \alpha^{-1})$, where α is the amplification number:

$$T = (1 - \alpha^{-1})\left[\hat{M}(\theta)\ddot{\theta} + \hat{C}(\theta, \dot{\theta})\dot{\theta}\right] + \hat{P}(\theta). \tag{5}$$

$\hat{M}(\theta)$, $\hat{C}(\theta, \dot{\theta})$ and $\hat{P}(\theta)$ are the estimates of the inertia matrix, the Coriolis matrix and the gravity vector, respectively, for the system shown in Fig. 4. Note that (5) results in a 7×1 actuator torque. Since there is no actuator between the BLEEX foot and the ground, the torque prescribed by the first element of T must be provided by the pilot. Substituting T from (5) into (3) yields:

$$M(\theta)\ddot{\theta} + C(\theta, \dot{\theta})\dot{\theta} + P(\theta) = (1 - \alpha^{-1})\left[\hat{M}(\theta)\ddot{\theta} + \hat{C}(\theta, \dot{\theta})\dot{\theta}\right] + \hat{P}(\theta) + d. \tag{6}$$

In the limit when $\hat{M}(\theta) = M(\theta)$, $\hat{C}(\theta, \dot{\theta}) = C(\theta, \dot{\theta})$, $\hat{P}(\theta) = P(\theta)$ and α is sufficiently large, d will approach zero, meaning the pilot can walk as if BLEEX did not exist. However, it can be seen from (6) that the force felt by the pilot is a function of α, and the accuracy of the estimates $\hat{M}(\theta)$, $\hat{C}(\theta, \dot{\theta})$ and $\hat{P}(\theta)$. In general, the more accurately the system is modeled, the less the human force, d, will be. The accuracy of this model is dependent upon the accuracy of the model parameters for the mass, inertia, centre of gravity location and geometry of each link.

2.4. Double support

In the double-support phase, both BLEEX feet are flat on the ground. The exoskeleton is modeled as two planar 3-d.o.f. serial link mechanisms that are connected to each other along their uppermost link (i.e., the torso) as shown in Fig. 5a. The dynamics for these serial links are represented by the equations:

$$M_{\text{L}}(m_{\text{TL}}, \theta_{\text{L}})\ddot{\theta}_{\text{L}} + C_{\text{L}}(m_{\text{TL}}, \theta_{\text{L}}, \dot{\theta}_{\text{L}})\dot{\theta}_{\text{L}} + P_{\text{L}}(m_{\text{TL}}, \theta_{\text{L}}) = T_{\text{L}} + d_{\text{L}}, \tag{7}$$

$$M_{\text{R}}(m_{\text{TR}}, \theta_{\text{R}})\ddot{\theta}_{\text{R}} + C_{\text{R}}(m_{\text{TR}}, \theta_{\text{R}}, \dot{\theta}_{\text{R}})\dot{\theta}_{\text{R}} + P_{\text{R}}(m_{\text{TR}}, \theta_{\text{R}}) = T_{\text{R}} + d_{\text{R}}, \tag{8}$$
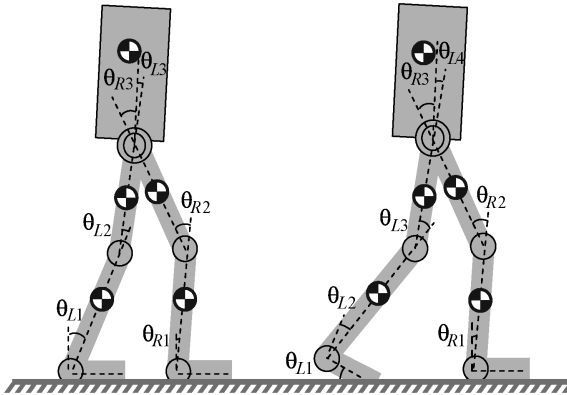

Figure 5. Sagittal plane representation of BLEEX in the double-support phase (left) and the double-support phase with one redundancy (right).

where:

$$\theta_L = \begin{bmatrix} \theta_{L1} \\ \theta_{L2} \\ \theta_{L3} \end{bmatrix}, \quad \theta_R = \begin{bmatrix} \theta_{R1} \\ \theta_{R2} \\ \theta_{R3} \end{bmatrix}. \tag{9}$$

m_{TL} and m_{TR} are effective torso masses supported by each leg, and m_T is the total torso mass such that:

$$m_T = m_{TL} + m_{TR}. \tag{10}$$

The contributions of m_T on each leg (i.e. m_{TL} and m_{TR}) are chosen as functions of the location of the torso center of gravity relative to the locations of the ankles such that:

$$\frac{m_{TR}}{m_{TL}} = \frac{x_{TL}}{x_{TR}}, \tag{11}$$

where x_{TL} is the horizontal distance between the torso center of gravity and the left ankle, and x_{TR} is the horizontal distance between the torso center of gravity and the right ankle. For example, if the center of gravity of the torso is located directly above the right leg, then $m_{TL} = 0$ and $m_{TR} = m_T$. Similar to the single-stance phase, the controllers are chosen such that:

$$T_L = (1 - \alpha^{-1})\left[\hat{M}_L(m_{TL}, \theta_L)\ddot{\theta}_L + \hat{C}_L(m_{TL}, \theta_L, \dot{\theta}_L)\dot{\theta}_L\right] + \hat{P}_L(m_{TL}, \theta_L), \tag{12}$$

$$T_R = (1 - \alpha^{-1})\left[\hat{M}_R(m_{TR}, \theta_R)\ddot{\theta}_R + \hat{C}_R(m_{TR}, \theta_R, \dot{\theta}_R)\dot{\theta}_R\right] + \hat{P}_R(m_{TR}, \theta_R). \tag{13}$$

Needless to say, (11) is valid only for quasi-static conditions where the accelerations and velocities are small. This is in fact the case, since in the double-support phase both legs are on the ground, and BLEEX's angular acceleration and velocities are quite small.

2.5. Double support with one redundancy

Double support with one redundancy is modeled as a 3-d.o.f. serial link mechanism for the stance leg with the foot flat on the ground and a 4-d.o.f. serial link mechanism for the stance leg that is not completely on the ground (Fig. 5b). Each serial link supports a portion of the torso weight. The dynamics for these serial links are similar to (7) and (8), with the exception that the redundant leg equation represents 4 as opposed to 3 d.o.f. For the specific instant shown in Fig. 5b, the left leg has 4 d.o.f. and the right leg has 3 d.o.f.

Similar to the double-support case, the effective torso mass supported by each leg is computed by (11). Controllers for this case can be chosen in the same manner as (12) and (13). Note that the actuator torque vector associated with the leg that has 4 d.o.f. (e.g. T_L for the case shown in Fig. 5b) is a 4 × 1 vector. As in the single-support phase, the torque prescribed by the first element of T must be provided by the pilot because there is no actuator between the BLEEX foot and the ground. As

the pilot walks, BLEEX transitions through the various phases shown in Fig. 3. The foot sole pressure sensors detect which leg has 4 d.o.f. and which leg has 3 d.o.f., and the controller then chooses the appropriate algorithm for each leg.

3. EXOSKELETON DYNAMICS

3.1. Three-segment model

For the purposes of the system identification experiments in this article, a simplified case of the dynamics will be considered in which the two legs have just 3 d.o.f.: a hip joint, a knee joint and an ankle joint (each of which is actuated within the sagittal plane by a hydraulic piston commanded by the controller). Only the dynamics of the leg while in swing mode will be investigated, so the torso can be regarded as being in a fixed position.

Each leg of the exoskeleton can be modeled as a two-dimensional three-segment manipulator, as described in Ref. [15]. A diagram of the simplified model is shown in Fig. 6. The length of the thigh link is L_t and the length of the shank link is L_s. The position of the center of gravity of the thigh is given by L_{G_t} and h_{G_t}, that of the shank by L_{G_s} and h_{G_s}, and that of the foot by L_{G_f} and h_{G_f}, as shown.

The joint angles θ_5, θ_6 and θ_7 are defined as shown. If all joint angles are zero, then the thigh and shank are vertical, and the foot is horizontal. The joint angle is positive if the angle of the lower link relative to the upper link is anti-clockwise.
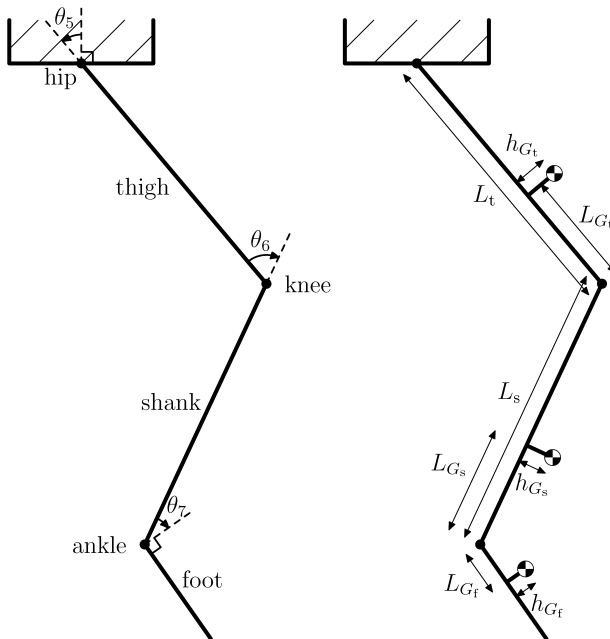

Figure 6. Three-segment model of the exoskeleton leg.

At each joint, there will be a torque acting between the two links. The torque T_5 acts between the torso and the thigh, the torque T_6 acts between the thigh and the shank, and the torque T_7 acts between the shank and the foot. The sign convention is such that a positive torque T_i will cause a positive acceleration $\ddot{\theta}_i$.

The masses of the thigh, shank and foot links are m_t, m_s and m_f, respectively. The moments of inertias of the links about their centres of gravity are I_t, I_s and I_f.

3.2. Ideal equations of motion

The derivation of the equations of motion for the simplified model of the exoskeleton leg is discussed in Ref. [15]. It is assumed that the only forces acting on the links are the joint torques, T_5, T_6 and T_7, and gravitational forces. Then expressions can be found for T_5, T_6 and T_7 in terms of the joint angles, $(\theta_5, \theta_6, \theta_7)$, the joint velocities, $(\dot{\theta}_5, \dot{\theta}_6, \dot{\theta}_7)$, the joint accelerations, $(\ddot{\theta}_5, \ddot{\theta}_6, \ddot{\theta}_7)$, and the constant geometry and mass parameters of the three links, $(L_t, L_s, L_{G_t}, h_{G_t}, L_{G_s}, h_{G_s}, L_{G_f}, h_{G_f}, m_t, m_s, m_f, I_t, I_s, I_f)$.

The lengths of the thigh and shank links, L_t and L_s, may be determined by direct measurement of the distances between the centers of the joints, so these parameters are known.

The form of the equations in Ref. [15] are unsuitable for use in system identification, as it can be shown that the parameters appearing in those equations cannot be determined experimentally. The equations will be rewritten here in terms of the following nine new parameters:

$$X_7 = -m_f h_{G_f}, \tag{14}$$
$$Y_7 = m_f L_{G_f}, \tag{15}$$
$$X_6 = m_s(L_s - L_{G_s}) + m_f L_s, \tag{16}$$
$$Y_6 = m_s h_{G_s}, \tag{17}$$
$$X_5 = m_t(L_t - L_{G_t}) + m_s L_t + m_f L_t, \tag{18}$$
$$Y_5 = m_t h_{G_t}, \tag{19}$$
$$J_7 = I_f + m_f(h_{G_f}^2 + L_{G_f}^2), \tag{20}$$
$$J_6 = J_7 + I_s + m_s\big((L_s - L_{G_s})^2 + h_{G_s}^2\big) + m_f L_s^2, \tag{21}$$
$$J_5 = J_6 + I_t + m_t\big((L_t - L_{G_t})^2 + h_{G_t}^2\big) + m_s L_t^2 + m_f L_t^2. \tag{22}$$

Then the dynamic equations for the leg in swing mode can be rewritten in terms of these nine new parameters. The torque equation for the ankle joint is:

$$
\begin{aligned}
T_7 = {} & \big[J_7 + L_s(X_7 \cos\theta_7 - Y_7 \sin\theta_7) + L_t(X_7 \cos\theta_{67} - Y_7 \sin\theta_{67})\big]\ddot{\theta}_5 \\
& + \big[J_7 + L_s(X_7 \cos\theta_7 - Y_7 \sin\theta_7)\big]\ddot{\theta}_6 + [J_7]\ddot{\theta}_7 \\
& + L_t(X_7 \sin\theta_{67} + Y_7 \cos\theta_{67})\,\dot{\theta}_5^2 \\
& + L_s(X_7 \sin\theta_7 + Y_7 \cos\theta_7)\,\dot{\theta}_{56}^2 \\
& + g(X_7 \sin\theta_{567} + Y_7 \cos\theta_{567}).
\end{aligned} \tag{23}
$$

Note that θ_{56} denotes $\theta_5 + \theta_6$, θ_{67} denotes $\theta_6 + \theta_7$ and θ_{567} denotes $\theta_5 + \theta_6 + \theta_7$. Similarly, $\dot{\theta}_{56}$ denotes $\dot{\theta}_5 + \dot{\theta}_6$ and so on.

The torque equation for the knee joint is:

$$
\begin{aligned}
T_6 = {} & \big[J_6 + 2L_s(X_7\cos\theta_7 - Y_7\sin\theta_7) + L_t(X_7\cos\theta_{67} - Y_7\sin\theta_{67}) \\
& + L_t(X_6\cos\theta_6 - Y_6\sin\theta_6)\big]\ddot{\theta}_5 \\
& + \big[J_6 + 2L_s(X_7\cos\theta_7 - Y_7\sin\theta_7)\big]\ddot{\theta}_6 \\
& + \big[J_7 + L_s(X_7\cos\theta_7 - Y_7\sin\theta_7)\big]\ddot{\theta}_7 \\
& + L_t(X_6\sin\theta_6 + Y_6\cos\theta_6)\,\dot{\theta}_5^2 \\
& + L_t(X_7\sin\theta_{67} + Y_7\cos\theta_{67})\,\dot{\theta}_5^2 \\
& + L_s(X_7\sin\theta_7 + Y_7\cos\theta_7)\big(\dot{\theta}_{56}^2 - \dot{\theta}_{567}^2\big) \\
& + g(X_6\sin\theta_{56} + Y_6\cos\theta_{56} + X_7\sin\theta_{567} + Y_7\cos\theta_{567}).
\end{aligned}
\tag{24}
$$

Finally, the torque equation for the hip joint is:

$$
\begin{aligned}
T_5 = {} & \big[J_5 + 2L_s(X_7\cos\theta_7 - Y_7\sin\theta_7) + 2L_t(X_7\cos\theta_{67} - Y_7\sin\theta_{67}) \\
& + 2L_t(X_6\cos\theta_6 - Y_6\sin\theta_6)\big]\ddot{\theta}_5 \\
& + \big[J_6 + 2L_s(X_7\cos\theta_7 - Y_7\sin\theta_7) + L_t(X_7\cos\theta_{67} - Y_7\sin\theta_{67}) \\
& + L_t(X_6\cos\theta_6 - Y_6\sin\theta_6)\big]\ddot{\theta}_6 \\
& + \big[J_7 + L_s(X_7\cos\theta_7 - Y_7\sin\theta_7) + L_t(X_7\cos\theta_{67} - Y_7\sin\theta_{67})\big]\ddot{\theta}_7 \\
& + L_t(X_6\sin\theta_6 + Y_6\cos\theta_6)\big(\dot{\theta}_5^2 - \dot{\theta}_{56}^2\big) \\
& + L_t(X_7\sin\theta_{67} + Y_7\cos\theta_{67})\big(\dot{\theta}_5^2 - \dot{\theta}_{567}^2\big) \\
& + L_s(X_7\sin\theta_7 + Y_7\cos\theta_7)\big(\dot{\theta}_{56}^2 - \dot{\theta}_{567}^2\big) \\
& + g(X_5\sin\theta_5 + Y_5\cos\theta_5 + X_6\sin\theta_{56} + Y_6\cos\theta_{56} + X_7\sin\theta_{567} \\
& + Y_7\cos\theta_{567}).
\end{aligned}
\tag{25}
$$

It can be shown that these nine parameters, X_7, Y_7, X_6, Y_6, X_5, Y_5, J_7, J_6 and J_5, are independent and can therefore be identified via experiment. They are a minimal set of parameters which fully describe the dynamics of the system.

Note that these equations apply to the case where the torso is stationary, which is the case for all experiments described in this report. However, if the dynamic equations are re-derived for the case when the torso is in motion, they can also be expressed in terms of only this reduced set of nine parameters. Therefore, it is still sufficient to identify only these parameters.

3.3. Friction, stiffness and damping

Let A_i denote the torque exerted on the joint by the hydraulic actuator. An accurate estimate of this torque can be obtained from the force sensor measurement and the joint angle encoder measurement (the joint angle is required to calculate the moment arm of the actuator force about the joint).

There are several other torques acting on the joint. We divide these into three components: a stiffness torque, a damping and kinetic friction torque, and a static friction torque. The stiffness torque, which we denote by B_i, is expected to be a function only of the joint angle, i.e., $B_i = b_i(\theta_i)$. The damping and kinetic friction torque, which we denote by C_i, is expected to be a function only of the joint angular velocity, i.e., $C_i = c_i(\dot{\theta}_i)$. This torque C_i is zero when $\dot{\theta}_i$ is zero. Finally, the static friction torque is denoted by D_i.

The total torque exerted on the joint is then given by:

$$T_i = A_i + B_i + C_i + D_i. \tag{26}$$

3.4. Parameters for identification

In order to have an accurate model of the relationship between the actuator torques and the motion of the exoskeleton, all terms in the equations above must be characterized.

The following parameters are known:

- Link lengths, L_t, L_s.
- Gravitational constant, g.

The terms which need to be identified are:

- Mass moment parameters, X_7, Y_7, X_6, Y_6, X_5, Y_5.
- Inertial parameters, J_7, J_6, J_5.
- Stiffness torques, B_7, B_6, B_5.
- Damping and kinetic friction torques, C_7, C_6, C_5.

The static friction torques, D_7, D_6, D_5, will not be characterised, for reasons described later.

4. PARAMETER IDENTIFICATION

4.1. Least-squares estimation

Least-squares estimation can be used to identify parameters in systems when we have a linear relationship between the unknown parameters with coefficients which are known functions of measurable quantities [16–20]. For example, suppose we have a system governed by:

$$y(t) = [\boldsymbol{h}(t)]^{\mathrm{T}} \boldsymbol{x}. \tag{27}$$

Here, $\boldsymbol{x}$ is a vector of n constant unknown parameters, $y(t)$ is the output of the system at time t, and the n coefficients in the vector $\boldsymbol{h}(t)$ are time-varying and depend upon the state of the system. However, we can determine $\boldsymbol{h}(t)$ from measurable quantities.

To estimate the unknown parameters, we take measurements $y(t_i)$ of the system output at m different times or configurations. At each of these times or configurations, we calculate the coefficients vector, $\boldsymbol{h}(t_i)$. Additionally, some noise $v(t_i)$ is introduced into each measurement, so that $y(t_i) = [\boldsymbol{h}(t_i)]^\mathrm{T}\boldsymbol{x} + v(t_i)$. Then, we can write these m equations in matrix form:

$$\boldsymbol{y} = H\boldsymbol{x} + \boldsymbol{v}, \tag{28}$$

where:

$$\boldsymbol{y} = \begin{bmatrix} y(t_1) \\ y(t_2) \\ \vdots \\ y(t_m) \end{bmatrix}, \quad \boldsymbol{v} = \begin{bmatrix} v(t_1) \\ v(t_2) \\ \vdots \\ v(t_m) \end{bmatrix}, \quad H = \begin{bmatrix} [\boldsymbol{h}(t_1)]^\mathrm{T} \\ [\boldsymbol{h}(t_2)]^\mathrm{T} \\ \vdots \\ [\boldsymbol{h}(t_m)]^\mathrm{T} \end{bmatrix}. \tag{29}$$

Then we can find a least-squares estimate $\hat{\boldsymbol{x}}$ using:

$$\hat{\boldsymbol{x}} = \left(H^\mathrm{T}H\right)^{-1}H^\mathrm{T}\boldsymbol{y}. \tag{30}$$

4.2. Experimental procedure

In this section, the experimental procedures followed in collecting data for the parameter identification process are outlined.

4.2.1. Static experiments. The static experiments are those in which the joint torques are measured when the exoskeleton is in a static configuration, so all joint velocities and accelerations are zero. For each experiment, the exoskeleton is placed on a jig so that the torso is held in the air at a fixed position and in vertical orientation. A sequence of configurations is programmed into the exoskeleton controller. Each configuration consists of a list of six joint angles, $(\theta_{5_\mathrm{L}}, \theta_{6_\mathrm{L}}, \theta_{7_\mathrm{L}}, \theta_{5_\mathrm{R}}, \theta_{6_\mathrm{R}}, \theta_{7_\mathrm{R}})$. When the controller is activated, the six actuators are each commanded to move the joint to the desired angle, θ_d.

The voltage sent to the actuators, u, is determined by a simple proportional controller, $u = -K_P(\theta - \theta_\mathrm{d})$, where θ is the joint angle measured by the encoder. After the joints have stopped moving, the data from each of the force sensors are collected. The joint angles measured by the encoders are also recorded. From these values, the torque exerted by the actuator at each of the six joints is calculated and recorded.

4.2.2. Dynamic experiments. In the dynamic experiments, the joint torques are measured when the exoskeleton is in motion. A trajectory of the robot configuration is programmed into the exoskeleton controller. The trajectory consists of a list of six joint angle trajectories, $(\theta_{5_\mathrm{L}}(t), \theta_{6_\mathrm{L}}(t), \theta_{7_\mathrm{L}}(t), \theta_{5_\mathrm{R}}(t), \theta_{6_\mathrm{R}}(t), \theta_{7_\mathrm{R}}(t))$. When the controller is activated, the six actuators are each commanded to track the desired trajectory, $\theta_\mathrm{d}(t)$. As in the static experiments, a simple proportional controller is used to determine the voltage sent to the actuators.

The joint encoder and force sensor readings are recorded at a rate of $f_s \approx 50$ Hz. At each sample point, the torque exerted by the actuator at each of the six joints is calculated from the joint encoder and force sensor readings and recorded.

After the experiment, the joint velocities and accelerations at each of the sample points (excepting the first and last) are estimated by finite difference approximations.

4.3. Static friction torques

When a robot leg is moved to a static configuration, $(\theta_5, \theta_6, \theta_7)$, the actuator torque for each joint depends on the direction from which the joint angle was reached. This phenomenon can be observed in the plot shown in Fig. 7. The hip and knee angles were held constant throughout this experiment. The ankle was moved cyclically through the angles $\{-15°, 0°, 15°, 0°\}$. On the actuator torque plot, the circles represent the torques A_7^+ where the angle position, $0°$, was approached from the negative and the crosses represent the torques A_7^- where the angle position was approached from the positive. It can be seen that the torques A_7^+ are consistently greater than the torques A_7^-.

The discrepancy between A_i^+ and A_i^- is due to the static friction torque, D_i. When the joint is moving with positive velocity (θ_i increasing), there is a negative kinetic friction torque to oppose the motion. When the joint comes to rest, there remains a negative static friction torque. If the joint comes to rest from the other direction, the static friction torque will be positive.
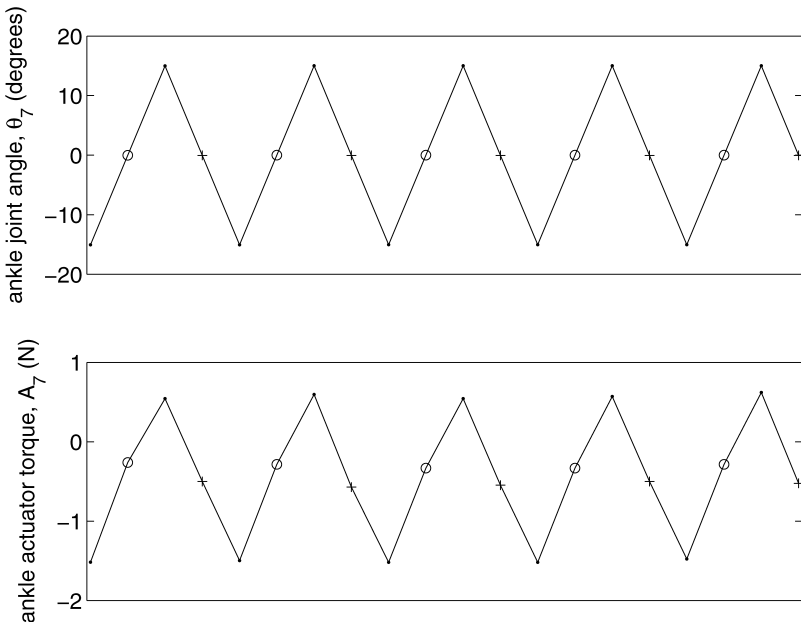

Figure 7. Effect of the static friction torque in the ankle.

When the robot is walking, no joint will be completely static. Therefore, the controller does not need to be able to estimate the static friction torque, so there is no reason to characterize it. However, in order to obtain accurate results in the estimation of the other parameters, it is desirable to reduce the effects of the static friction torques. This can be achieved by taking each static torque measurement twice, first approaching the the joint angle θ_i from the negative direction, then approaching it from the positive direction. The two torques obtained, A_i^+ and A_i^-, are then averaged to obtain an estimate of what the actuator torque would be if there were no static friction torque.

4.4. Stiffness torques

When the robot is static ($\dot{\theta}_5 = \dot{\theta}_6 = \dot{\theta}_7 = 0$ and $\ddot{\theta}_5 = \ddot{\theta}_6 = \ddot{\theta}_7 = 0$), the ankle joint torque given by (23) becomes:

$$T_7 = g\left(X_7 \sin \theta_{567} + Y_7 \cos \theta_{567}\right). \tag{31}$$

Also, under static conditions, the damping and kinetic friction torque, C_7, is zero. We eliminate the static friction torque, D_7, by averaging two measurements as discussed in the previous section. Therefore, from (26), when the robot is static, the measured torque is:

$$A_7 = g\left(X_7 \sin \theta_{567} + Y_7 \cos \theta_{567}\right) - B_7. \tag{32}$$

To identify the ankle stiffness torque, B_7, the robot was controlled to move to a series of positions such that θ_{567} was the same at each of the positions, while θ_5, θ_6 and θ_7 were all varied. Then the term $(X_7 \sin \theta_{567} + Y_7 \cos \theta_{567})$ is constant for the set of positions, so the measured torque is:

$$A_7 = -B_7 + g\left(X_7 \sin \theta_{567} + Y_7 \cos \theta_{567}\right), \tag{33}$$

where $g(X_7 \sin \theta_{567} + Y_7 \cos \theta_{567})$ is a constant.

The measured torque, A_7, was plotted against the ankle joint angle, θ_7. The experiment was repeated for several different values of θ_{567}. The different data sets were found to have the same shape, as shown in Fig. 8, supporting the assumption that B_7 is a function only of θ_7, so we can write $B_7 = b_7(\theta_7)$.

It was found that a quadratic function, $b_{27}\theta_7^2 + b_{17}\theta_7 + c$, fit the resulting plots very closely. The parameters b_{27} and b_{17} were determined using a least squares fit. Then our characterization of the stiffness function is:

$$b_7(\theta_7) = b_{27}\theta_7^2 + b_{17}\theta_7 + b_{07}. \tag{34}$$

However, the parameter b_{07} could not be determined from the previous data alone, since the constants $g(X_7 \sin \theta_{567} + Y_7 \cos \theta_{567})$ for each value of θ_{567} were unknown.

In order to find the parameter b_{07}, the robot was controlled to two positions, $(\theta_5, \theta_6, \theta_7)$ and $(\theta_5', \theta_6', \theta_7')$, such that $\theta_5' + \theta_6' = \theta_5 + \theta_6 + 180°$ and $\theta_7' = \theta_7$. The
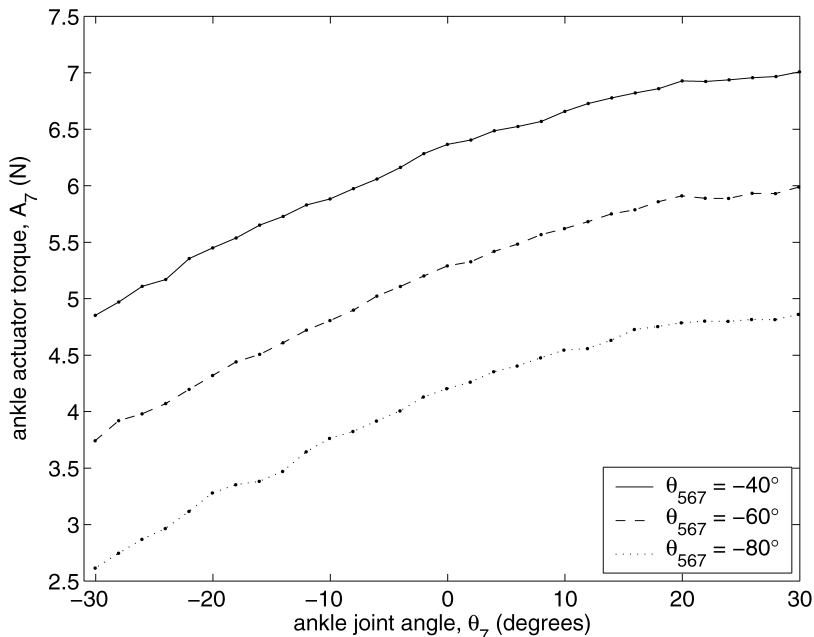
Figure 8. Effects of the stiffness torque in the ankle for various values of θ_{567}.

measured torques are:

$$A_7 = -b_7(\theta_7) + g\left(X_7 \sin\theta_{567} + Y_7 \cos\theta_{567}\right), \qquad (35)$$

$$A'_7 = -b_7(\theta'_7) + g\left(X_7 \sin\theta'_{567} + Y_7 \cos\theta'_{567}\right). \qquad (36)$$

Since $\theta'_{567} = \theta_{567} + 180°$, it can be shown that:

$$b_7(\theta_7) = -\frac{A_7 + A'_7}{2}. \qquad (37)$$

Therefore, from these two torque measurements, and using our previously determined values of b_{27} and b_{17}, we obtain an estimate of b_{07}:

$$b_{07} = -\frac{A_7 + A'_7}{2} - b_{27}\theta_7^2 - b_{17}\theta_7. \qquad (38)$$

By taking a large number of pairs of torque measurements of this kind and averaging the resulting values of b_{07}, we can determine b_{07}.

The procedure for identifying the stiffness torque in the knee joint is very similar. As for the ankle, we find that the knee actuator torques are dependent only on the knee joint angle, so $B_6 = b_6(\theta_6)$. Our characterization of the stiffness function is:

$$b_6(\theta_6) = b_{26}\theta_6^2 + b_{16}\theta_6 + b_{06}, \qquad (39)$$

and the three parameters b_{26}, b_{16} and b_{06} are identified.

Finding the stiffness torque in the hip joints is much more difficult than finding the stiffness torques in the knee and ankle joints. In principle, a method similar to those used for the knee and ankle joints could be used, but this would require experiments with the exoskeleton torso mounted in many different orientations, so that the hip joint angle would change while the gravitational torque on the hip remained constant.

There is no reason that the magnitude of the stiffness torque in the hip joints should be greater (or smaller) than that in the knee and ankle joints. However, the total torque in the hip joint is in general significantly greater in magnitude than that in the knee and ankle joints. Therefore, the relative impact of the stiffness torque on the total torque is much less significant in the hip joint than in the other joints.

For these reasons, the stiffness torque in the hip joints was not identified. The best estimate without experimental data is $B_5 = 0$.

4.5. Mass moment parameters

Equation (32) is the ankle torque equation under static conditions. Substituting in (34) for the ankle stiffness torque and rearranging yields:

$$g(X_7 \sin \theta_{567} + Y_7 \cos \theta_{567}) = A_7 + (b_{27}\theta_7^2 + b_{17}\theta_7 + b_{07}). \tag{40}$$

The robot is controlled to move to a series of 100 static configurations, and the joint angles and the ankle joint torque are measured at each one. Then, for each configuration, the right-hand side of (40), $A_7 + b_{27}\theta_7^2 + b_{17}\theta_7 + b_{07}$, is known, because the parameters b_{27}, b_{17} and b_{07} have been identified. Additionally, on the left-hand side, the gravitational constant g is known, and the values $\sin \theta_{567}$ and $\cos \theta_{567}$ can be calculated. Therefore, we can use a least-squares fitting to estimate X_7 and Y_7 from these measurements.

We can find the knee and hip mass moment parameters in an identical manner.

4.6. Inertia parameters

4.6.1. Foot inertia parameter. When the ankle and hip joints are stationary ($\ddot{\theta}_5 = \ddot{\theta}_7 = 0$, $\dot{\theta}_5 = \dot{\theta}_7 = 0$), then the torque equation for the ankle joint is:

$$T_7 = \left[J_7 + L_s(X_7 \cos \theta_7 - Y_7 \sin \theta_7)\right]\ddot{\theta}_6 + L_s(X_7 \sin \theta_7 + Y_7 \cos \theta_7)\,\dot{\theta}_6^2 \\ + g(X_7 \sin \theta_{567} + Y_7 \cos \theta_{567}). \tag{41}$$

Neglecting the friction torque, D_7, which is small compared to the total dynamic ankle torque, the left-hand side of this equation is equal to $A_7 + B_7 + C_7$. We know $C_7 = 0$, since $\dot{\theta}_7 = 0$. Therefore, we have:

$$\left[J_7 + L_s(X_7 \cos \theta_7 - Y_7 \sin \theta_7)\right]\ddot{\theta}_6 \\ = A_7 + B_7 - L_s(X_7 \sin \theta_7 + Y_7 \cos \theta_7)\,\dot{\theta}_6^2 - g(X_7 \sin \theta_{567} + Y_7 \cos \theta_{567}), \tag{42}$$
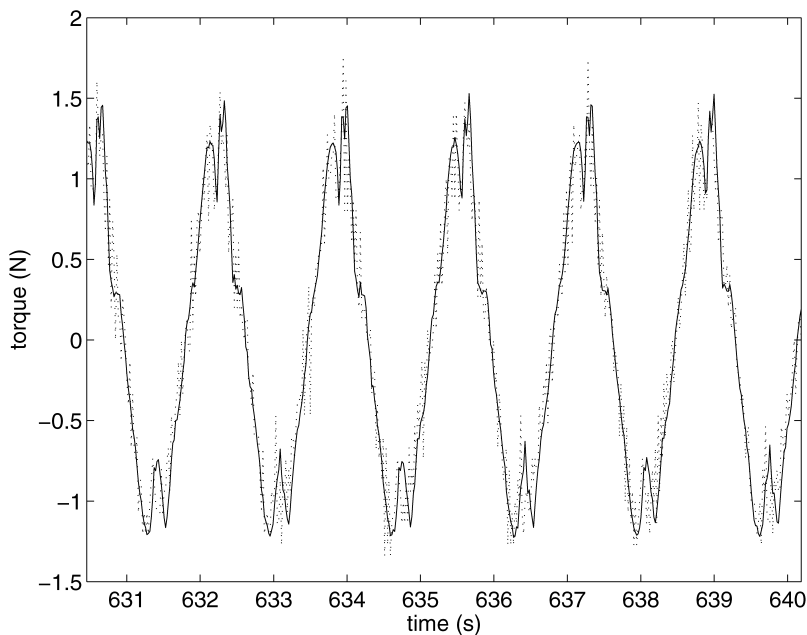
Figure 9. The inertial component of the ankle joint torque.

where the right-hand side of the equation is known, since X_7 and Y_7 have been identified. The only unknown is the foot inertia parameter, J_7. The coefficient of $\ddot{\theta}_6$ is a constant, since the ankle joint angle θ_7 is fixed.

To identify the parameter J_7, the hip and ankle joints were controlled to fixed positions, while the knee joint was controlled to track a sinusoidal input of fixed frequency. The joint angles and ankle joint torque were recorded. This was repeated for five different frequencies (0.2, 0.4, 0.6, 0.8 and 1.0 Hz).

A least-squares fitting was then used to estimate the value of $[J_7 + L_s(X_7 \cos \theta_7 - Y_7 \sin \theta_7)]$ from this data. Finally, the known values of L_s, X_7 and Y_7, along with the constant value of θ_7 for the experiments, were used to obtain an estimate of the foot inertia parameter, J_7.

A plot of the fit for one of the experiments is shown in Fig. 9. The solid line shows the right-hand side of (42) calculated from the torque and joint angle measurements. The dotted line shows the left-hand side of (42) calculated using the the value of J_7 obtained from the least-squares fitting. The plots matched well for all of the experiments, verifying the form of the equation.

4.6.2. Shank inertia parameter.   When the ankle and knee joints are stationary ($\ddot{\theta}_6 = \ddot{\theta}_7 = 0$, $\dot{\theta}_6 = \dot{\theta}_7 = 0$), neglecting the friction torque, D_6, we have:

$$\begin{aligned}
&\big[J_6 + 2L_s(X_7 \cos \theta_7 - Y_7 \sin \theta_7) + L_t(X_7 \cos \theta_{67} - Y_7 \sin \theta_{67}) \\
&\quad + L_t(X_6 \cos \theta_6 - Y_6 \sin \theta_6)\big]\ddot{\theta}_5
\end{aligned}$$

$$= A_6 + B_6 - L_\mathrm{t}(X_6 \sin\theta_6 + Y_6 \cos\theta_6)\,\dot\theta_5^2 - L_\mathrm{t}(X_7 \sin\theta_{67} + Y_7 \cos\theta_{67})\,\dot\theta_5^2$$
$$- g(X_6 \sin\theta_{56} + Y_6 \cos\theta_{56} + X_7 \sin\theta_{567} + Y_7 \cos\theta_{567}), \tag{43}$$

where the right-hand side of the equation is known, since X_7, Y_7, X_6 and Y_6 have been identified. The only unknown is the shank inertia parameter, J_6. The coefficient of $\ddot\theta_5$ is a constant, since the knee and ankle joint angles θ_6 and θ_7 are fixed.

To identify the parameter J_6, the knee and ankle joints were controlled to fixed positions, while the hip joint was controlled to track a sinusoidal input of fixed frequency. The joint angles and ankle joint torque were recorded. This was repeated for five different frequencies (0.2, 0.4, 0.6, 0.8 and 1.0 Hz).

A least-squares fitting was then used to estimate the value of:

$$\big[J_6 + 2L_\mathrm{s}(X_7 \cos\theta_7 - Y_7 \sin\theta_7) + L_\mathrm{t}(X_7 \cos\theta_{67} - Y_7 \sin\theta_{67})$$
$$+ L_\mathrm{t}(X_6 \cos\theta_6 - Y_6 \sin\theta_6)\big],$$

from this data. Finally, the known values of L_s, L_t, X_7, Y_7, X_6 and Y_6, along with the constant values of θ_6 and θ_7 for the experiments, were used to obtain an estimate of the shank inertia parameter, J_6.

The results were verified by plotting the right-hand side of (43) calculated from the torque and joint angle measurements against the left-hand side calculated using the the value of J_6 obtained. Again, the plots matched well for all of the experiments, verifying the form of the equation.

4.6.3. Thigh inertia parameter. When the ankle and knee joints are stationary ($\ddot\theta_6 = \ddot\theta_7 = 0$, $\dot\theta_6 = \dot\theta_7 = 0$), neglecting both the friction torque, D_5, and the damping and kinetic friction torque C_5, we have:

$$\big[J_5 + 2L_\mathrm{s}(X_7 \cos\theta_7 - Y_7 \sin\theta_7) + 2L_\mathrm{t}(X_7 \cos\theta_{67} - Y_7 \sin\theta_{67}) + 2L_\mathrm{t}(X_6 \cos\theta_6$$
$$- Y_6 \sin\theta_6)\big]\ddot\theta_5$$
$$= A_5 - g(X_5 \sin\theta_5 + Y_5 \cos\theta_5 + X_6 \sin\theta_{56} + Y_6 \cos\theta_{56} + X_7 \sin\theta_{567}$$
$$+ Y_7 \cos\theta_{567}), \tag{44}$$

where the right-hand side of the equation is known, since X_7, Y_7, X_6, Y_6, X_5 and Y_5 have been identified. The only unknown is the thigh inertia parameter, J_5. The coefficient of $\ddot\theta_5$ is a constant, since the joint angles θ_6 and θ_7 are fixed.

To identify the parameter J_5, the ankle and knee joints were controlled to fixed positions, while the hip joint was controlled to track a sinusoidal input of fixed frequency. The joint angles and hip joint torque were recorded. This was repeated for five different frequencies (0.2, 0.4, 0.6, 0.8 and 1.0 Hz).

A least-squares fitting was then used to estimate the value of:

$$\big[J_5 + 2L_\mathrm{s}(X_7 \cos\theta_7 - Y_7 \sin\theta_7) + 2L_\mathrm{t}(X_7 \cos\theta_{67} - Y_7 \sin\theta_{67})$$
$$+ 2L_\mathrm{t}(X_6 \cos\theta_6 - Y_6 \sin\theta_6)\big],$$

from this data. Finally, the known values of L_s, L_t, X_7, Y_7, X_6 and Y_6, along with the constant values of θ_6 and θ_7 for the experiments, were used to obtain an estimate of the thigh inertia parameter, J_5.

The results were verified by plotting the right-hand side of (44) calculated from the torque and joint angle measurements against the left-hand side calculated using the the value of J_6 obtained. Again, the plots matched well for all of the experiments, verifying the form of the equation.

4.7. Damping and kinetic friction torques

When the hip and knee joints are stationary ($\ddot{\theta}_5 = \ddot{\theta}_6 = 0$, $\dot{\theta}_5 = \dot{\theta}_6 = 0$), then the torque equation for the ankle joint is:

$$T_7 = [J_7]\ddot{\theta}_7 + g(X_7 \sin\theta_{567} + Y_7 \cos\theta_{567}). \tag{45}$$

If the ankle joint is in motion, then the static friction torque, D_7, is zero. Then the left-hand side of this equation is equal to $A_7 + B_7 + C_7$. The actuator torque A_7 is measured and the stiffness torque B_7 can be calculated from the joint angle using the stiffness function $b_7(\theta_7)$ found in Section 4.4. Therefore, the right-hand side of the equation:

$$C_7 = [J_7]\ddot{\theta}_7 + g(X_7 \sin\theta_{567} + Y_7 \cos\theta_{567}) - A_7 - B_7, \tag{46}$$

is known. The damping and kinetic friction torque, C_7, is expected to be a function of the joint angular velocity, $C_7 = c_7(\dot{\theta}_7)$.

To find the damping and kinetic friction function, $c_7(\dot{\theta}_7)$, the hip and knee joints were controlled to fixed positions, while the ankle joint was controlled to track a sinusoidal input of fixed frequency. The joint angles and ankle joint torque were recorded. This was repeated for five different frequencies (0.2, 0.4, 0.6, 0.8 and 1.0 Hz).

The damping and kinetic friction torque, C_7, was calculated from (46). A plot of C_7 against the joint angular velocity, $\dot{\theta}_7$, for one of the experiments is shown in Fig. 10.

It can be seen that the torque C_7 is approximately proportional to $\text{sgn}\,\dot{\theta}_7$. The same result was found in all experiments. This shows that there is very little damping torque, which would be approximately proportional to $\dot{\theta}_7$. There is only a kinetic friction torque, of the form:

$$c_7(\dot{\theta}_7) = c_{07}\,\text{sgn}\,\dot{\theta}_7. \tag{47}$$

The constant of proportionality, c_{07}, was found using a least-squares fitting to the data from several different frequencies (data points with $\dot{\theta}_7$ close to 0 were discarded, due to the discontinuity in $\text{sgn}\,\dot{\theta}_7$).

The procedure for identifying the damping and kinetic friction torque in the knee joint is very similar. As for the ankle, we find that there is very little damping torque,
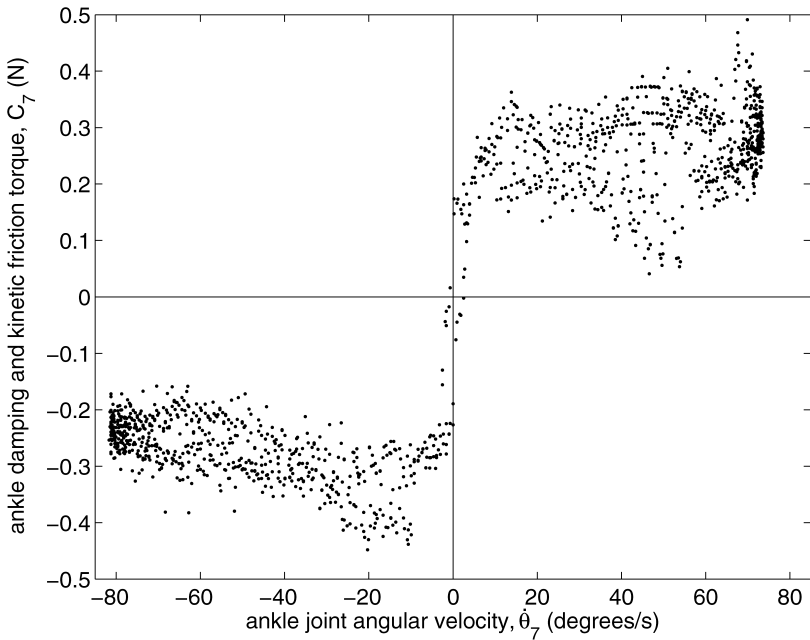
Figure 10. The ankle damping and kinetic friction torque, C_7.

but only a kinetic friction torque of the form:

$$c_6(\dot{\theta}_6) = c_{06} \operatorname{sgn} \dot{\theta}_6, \tag{48}$$

and the constant of proportionality, c_{06}, is identified.

However, the damping and kinetic friction torque in the hip joint was unable to be identified using the same method as was used to determine those in the ankle and knee joints, due to the larger errors in the identification of X_5, Y_5 and J_5.

It would be expected that the kinetic friction torques in the hip are the same order of magnitude as those in the knee and ankle joints. Since the total torque in the hip joint is in general significantly greater in magnitude than that in the knee and ankle joints, the relative impact of the kinetic friction torque on the total torque is much less significant in the hip joint than in the other joints.

For these reasons, the damping and kinetic friction torque in the hip joints was not identified. The best estimate without experimental data is $C_5 = 0$.

5. ANALYSIS OF RESULTS

5.1. Summary of numerical results

The numerical results of the identification experiments are presented in Tables 1–4. As discussed, the stiffness torques and the damping and kinetic friction torques in the hip joints were not identified. The best estimate of these torques without experimental data are $B_5 = 0$ and $C_5 = 0$.

Table 1.
Stiffness torques

Left leg

$B_7 = (0.3129 \, \text{N m/rad}^2) \, \theta_7^2 + (0.1557 \, \text{N m/rad}) \, \theta_7 + (-0.5829 \, \text{N m})$
$B_6 = (0.6263 \, \text{N m/rad}^2) \, \theta_6^2 + (1.9334 \, \text{N m/rad}) \, \theta_6 + (0.5 \, \text{N m})$

Right leg
$B_7 = (-1.5341 \, \text{N m/rad}^2) \, \theta_7^2 + (2.1484 \, \text{N m/rad}) \, \theta_7 + (4.5771 \, \text{N m})$
$B_6 = (1.2573 \, \text{N m/rad}^2) \, \theta_6^2 + (2.2442 \, \text{N m/rad}) \, \theta_6 + (-1.0 \, \text{N m})$

Table 2.
Mass moment parameters (kg m)

Left leg	Right leg
$X_7 = 0.2552$	$X_7 = 0.2554$
$Y_7 = 0.1313$	$Y_7 = 0.1279$
$X_6 = 1.9628$	$X_6 = 1.9532$
$Y_6 = 0.0031$	$Y_6 = -0.0386$
$X_5 = 3.9819$	$X_5 = 4.0474$
$Y_5 = -0.4083$	$Y_5 = -0.4990$

Table 3.
Inertia parameters (kg m^2)

Left leg	Right leg
$J_7 = 0.04528$	$J_7 = 0.05243$
$J_6 = 0.7833$	$J_6 = 0.7897$
$J_5 = 2.380$	$J_5 = 2.598$

Table 4.
Kinetic friction torques

Left leg	Right leg
$C_7 = -(0.2646 \, \text{N m}) \, \text{sgn} \, \dot{\theta}_7$	$C_7 = -(0.3370 \, \text{N m}) \, \text{sgn} \, \dot{\theta}_7$
$C_6 = -(0.5291 \, \text{N m}) \, \text{sgn} \, \dot{\theta}_6$	$C_6 = -(0.4081 \, \text{N m}) \, \text{sgn} \, \dot{\theta}_6$

Table 5.
SolidWorks parameters

$X_7 = 0.2793 \, \text{kg m}$	$X_6 = 2.055 \, \text{kg m}$	$X_5 = 3.783 \, \text{kg m}$
$Y_7 = 0.1546 \, \text{kg m}$	$Y_6 = 0.05778 \, \text{kg m}$	$Y_5 = -0.1601 \, \text{kg m}$
$J_7 = 0.05628 \, \text{kg m}^2$	$J_6 = 0.8939 \, \text{kg m}^2$	$J_5 = 2.497 \, \text{kg m}^2$

The mass moment parameters and inertia parameters can be compared to the values calculated by SolidWorks from the design models of the parts. The values are the same for the left and right legs, since the designs are identical. These are shown in Table 5.

5.2. Comparison of models

In order to evaluate the accuracy of the system model obtained from the system identification results, the exoskeleton was controlled to move each of its joints in a sinusoidal trajectory. The six actuator torques, A_i, were both measured *via* the force sensors, and estimated from the identified parameters and functions identified experimentally.

The estimates of the actuator torques calculated from the system identification results were compared to the actual measured actuator torques. One set of results is shown in the dark black lines of Fig. 11. It can be seen that the calculated actuator torques closely match the measured actuator torques. Therefore, the results of the system identification provide a good model of the dynamics.

The light grey lines in Fig. 11 show the estimates of the actuator torques calculated from the model based on the SolidWorks designs of the exoskeleton. It can be seen that, in general, this model is significantly less accurate than the results using the system identification based model.

6. CONCLUSIONS

In order to achieve a compliant control system for BLEEX, a very accurate model of the system dynamics is required. A series of system identification experiments was designed and carried out for BLEEX.

In order to fully characterize the relationship between the motion of the exoskeleton leg and the torques exerted by the hydraulic actuators, it is necessary to identify:

- Mass moment parameters, X_7, Y_7, X_6, Y_6, X_5, Y_5.
- Inertial parameters, J_7, J_6, J_5.
- Stiffness torques, B_7, B_6, B_5.
- Damping and kinetic friction torques, C_7, C_6, C_5.

Each of these terms was isolated individually in the equations of motion, and experiments were designed and performed to identify each of them in turn. Only the stiffness, damping and kinetic friction torques in the hip were not found, and these were judged to have a relatively small impact on the motion of the exoskeleton.

The results of the identification process produced an accurate model of the dynamics of the exoskeleton legs. This model was compared to the simplistic model predicted from the robot designs and was found to be much more accurate.
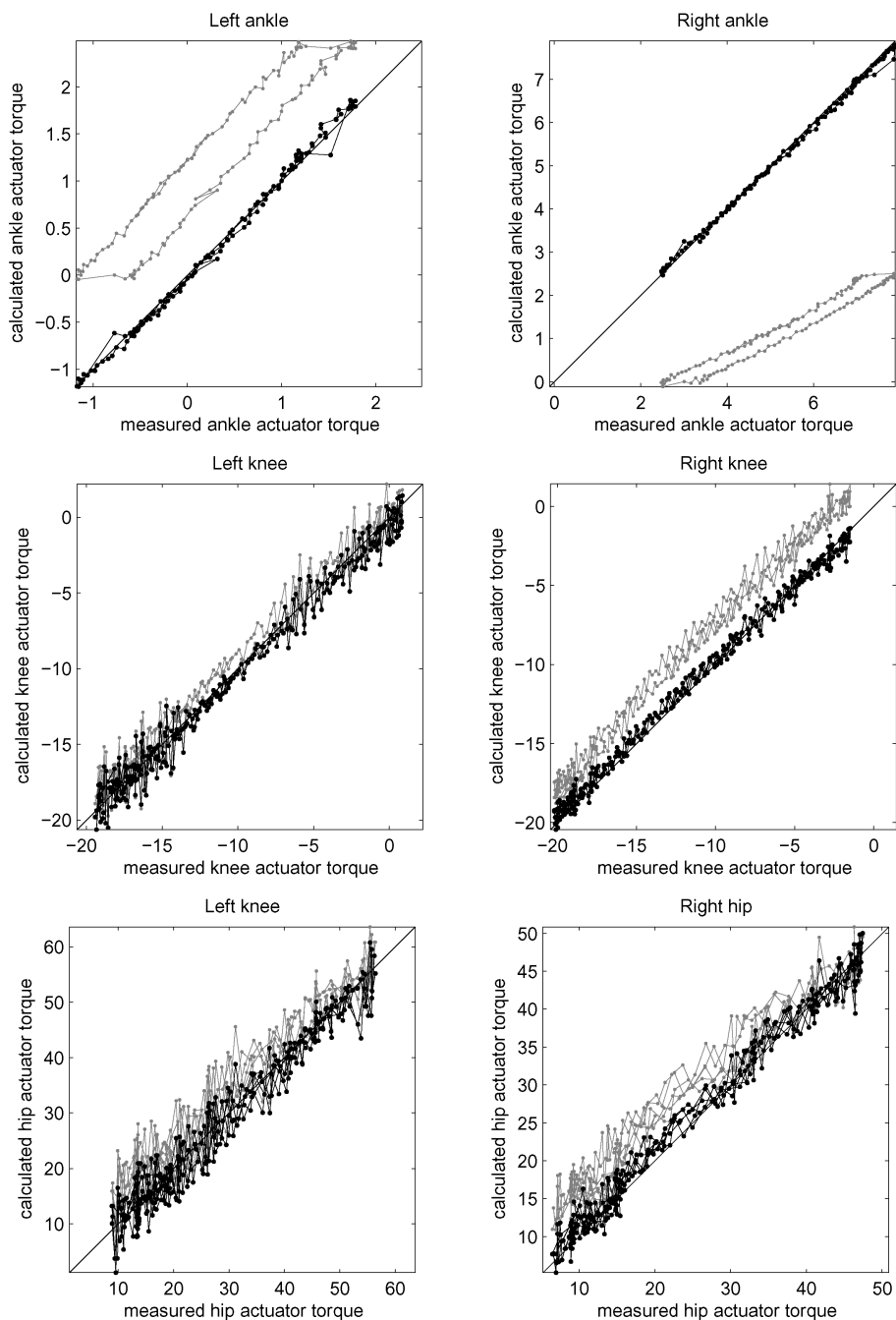
Figure 11. Comparison of calculated actuator torques to measured actuator torques in a dynamic experiment.

REFERENCES

1. H. Kazerooni, J. L. Racine, L. Huang and R. Steger, On the control of the Berkeley Lower Extremity Exoskeleton (BLEEX), in: *Proc. IEEE Int. Conf. Robotics and Automation*, Barcelona, pp. 4353–4360 (2005).
2. H. Kazerooni, Human–robot interaction via the transfer of power and information signals, *IEEE Trans. Syst. Cybernet.* **20**, 450–463 (1990).
3. H. Kazerooni and J. Guo, Human extenders, *J. Dyn. Syst. Meas. Control* **115**, 281–289 (1993).
4. H. Kazerooni and S. Mahoney, Dynamics and control of robotic systems worn by human, *J. Dyn. Syst. Meas. Control* **113**, 379–387 (1991).
5. H. Kazerooni and M. Her, The dynamics and control of a haptic interface device, *IEEE Trans. Robotics Automat.* **10**, 453–464 (1994).
6. H. Kazerooni and T. Snyder, A case study on dynamics of haptic devices: human induced instability in powered hand controllers, *AIAA J. Guid. Control Dyn.* **18** (1995).
7. H. Kazerooni and R. Steger, The Berkeley lower extremity exoskeleton, *J. Dyn. Syst. Meas. Control* **128**, 14–25 (2006).
8. A. Chu, H. Kazerooni and A. Zoss, On the biomimetic design of the Berkeley Lower Extremity Exoskeleton (BLEEX), in: *Proc. IEEE Int. Conf. Robotics and Automation*, Barcelona, pp. 4345–4352 (2005).
9. A. Zoss, H. Kazerooni and A. Chu, On the mechanical design of the Berkeley Lower Extremity Exoskeleton, in: *Proc. IEEE Int. Conf. on Intelligent Robots and Systems*, Edmonton, pp. 3465–3472 (2005).
10. K. Amundsen, J. Raade, N. Harding and H. Kazerooni, Hybrid hydraulic–electric power unit for field and service robots, in: *Proc. IEEE Int. Conf. on Intelligent Robots and Systems*, Edmonton, pp. 3453–3458 (2005).
11. T. McGee, J. Raade and H. Kazerooni, Monopropellant-driven free piston hydraulic pump for mobile robotic systems, *J. Dyn. Syst. Meas. Control* **126**, 75–81 (2004).
12. J. Raade and H. Kazerooni, Analysis and design of a novel power supply for mobile robots, in: *Proc. IEEE Int. Conf. Robotics and Automation*, New Orleans, LA, pp. 4911–4917 (2004).
13. S. Kim, G. Anwar and H. Kazerooni, High-speed communication network for controls with application on the exoskeleton, in: *Proc. Am. Control Conf.*, Boston, MA, pp. 350–360 (2004).
14. S. Kim and H. Kazerooni, High-speed ring-based distributed networked control system for real-time multivariable applications, in: *Proc. ASME Int. Mechanical Engineering Congr.*, Anaheim, CA (2004).
15. J. L. Racine, Control of a lower extremity exoskeleton for human performance amplification, PhD Dissertation, University of California, Berkeley, CA (2003).
16. T. C. Hsia, *System Identification*. Lexington Books, Lanham, MD (1977).
17. D. D. Joshi, *Linear Estimation and Design of Experiments*. Wiley, New York (1987).
18. T. Kariya and H. Kurata, *Generalized Least Squares*. Wiley, New York (2004).
19. C. R. Rao and H. Toutenberg, *Linear Models: Least Squares and Alternatives*, 2nd edn. Springer, Berlin (1999).
20. H. W. Sorenson, *Parameter Estimation (Control and Systems Theory Series)*. Dekker, New York (1980).

ABOUT THE AUTHORS
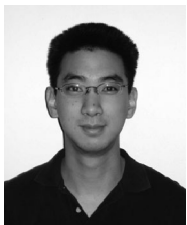
Justin Ghan received his B.S. in Mechatronics Engineering from the University of Adelaide (Australia) in 2002, and his M.S. in Mechanical Engineering from the University of California, Berkeley in 2005. His research was on the control of the Berkeley Lower Extremity Exoskeleton, with an emphasis on system identification. He is currently a Ph.D. student at the University of California, Berkeley.

Ryan Steger received his Ph.D. in Mechanical Engineering in 2006 from the University of California, Berkeley. His research focuses on the design and control of human exoskeletons for enhancing human performance and endurance. Ryan received his M.S. degree from U.C. Berkeley in 2003 and his B.S. degree from Rice University in 2001.

H. Kazerooni received the M.S. and Ph.D. degrees in mechanical engineering from the Massachusetts Institute of Technology, Cambridge, Massachusetts, in 1982 and 1984, respectively. He is currently a Professor in the Mechanical Engineering Department at the University of California, Berkeley and Director of the Robotics and Human Engineering Laboratory.